Nanoshells for Surface-Enhanced Raman Spectroscopy in Eukaryotic Cells: Cellular Response and Sensor Development

Michael A. Ochsenkühn,[†] Phillip R. T. Jess,[§] Helene Stoquert,[‡] Kishan Dholakia,[§] and Colin J. Campbell[†,‡,*]

[†]School of Chemistry, University of Edinburgh, Edinburgh EH9 3JJ, U.K., [‡]Division of Pathway Medicine, University of Edinburgh, EH16 5SB Edinburgh, U.K., and [§]SUPA, School of Physics and Astronomy, University of St. Andrews, St. Andrews Fife KY16 9SS, U.K.

ABSTRACT The application of gold nanoshells (NS) as a surface-enhanced Raman (SER) platform for intracellular sensing in NIH-3T3 fibroblast cells was studied by using a near-infrared Raman system. To show the feasibility of using these 151 ± 5 nm sized solution-stable nanoparticles inside living cells, we investigated the uptake, cellular response, and the health of the cell population. We show that NS are taken up voluntarily and can be found in the cytosol by transmission electron microscopy (TEM), which also provides detailed information about location and immediate surrounding of the NS. The internalization into cells has been found to be independent of active cellular mechanisms, such as endocytosis, and can be suggested to be of passive nature. Uptake of NS into cells can be controlled, and cells show no increase in necrosis or apoptosis as a result; we show that NS-based intracytosolic SER spectra can be measured on biological samples using short acquisition times and low laser powers. We demonstrate its application using 4-mercaptobenzoic acid (4-MBA)-functionalized nanoshells as a pH sensor.

KEYWORDS: nanoshells (NS) · surface-enhanced Raman spectroscopy · nanoparticle uptake · cell viability · cytotoxicity · nanosensors

Nanoparticles have found various applications in biomedical research.[1−5] They are used, for example, in drug delivery,[3,6] intracellular sensing,[7,8] and diagnosis and treatment of cancer.[9−14] In addition, the ubiquitous use of nanomaterials in everyday applications, such as waterproofing formulations, sun creams, and detergents, means that a thorough knowledge about their possible toxic effects is crucial.[15] For example, studies on long carbon nanotubes show that the hazardous potential on inhalation is comparable to asbestos,[16,17] a fibrous silicate material which was banned due to its toxicity over a decade ago. However, shorter (100 nm), conjugated carbon nanotubes have been shown to have no serious cytotoxicity in mammalian cells.[18]

Since our ultimate goal is to perform surface-enhanced Raman spectroscopic (SERS) studies to understand cellular behavior, we have started by investigating the effects of nanoparticle exposure on our biological model systems. Most studies on intracellular SERS have focused on collecting spectra and have stopped short of a thorough examination of the cellular response to the nanomaterial.[2,19,20] Furthermore, very few publications have taken the next step and examined the actual mechanism of particle uptake,[6,21−23] even though the impact on the disturbance caused inside the cells and therefore the applicability of the method is dependent on where, and in which state, we find the particles after internalization.

We report here the results of an investigation in the cellular uptake and response of cells to nanoshells (NS).[24,25] These core−shell particles consisting of a silica core of around 120 nm in diameter encapsulated in a thin and stable layer of gold exhibit absorbance which can be tuned to a necessary optical wavelength by the core−shell diameter ratio.[26] NS exhibit surface plasmon resonance (SPR), which can be excited by illumination with light of a suitable wavelength.[25,27−32] The SPR of NS enhances the inherently weak Raman signal of molecules in the near vicinity of the particle surface[33,34] and has been shown to enhance the Raman signal by a factor of 10^{12}.[35] Investigating the cell viability of murine 3T3/NIH fibroblasts in culture after NS incubation shows that the cells are viable, an observation which is supported by measuring markers of apoptosis and necrosis. Further, we have examined the fate of the NS inside the cells using transmission electron microscopy (TEM),[36] allowing us to locate and study the immediate surroundings of the particles. Finally, we show the difference

*Address correspondence to colin.campbell@ed.ac.uk.

Received for review June 26, 2009 and accepted September 22, 2009.

Published online October 6, 2009.
10.1021/nn900681c CCC: $40.75

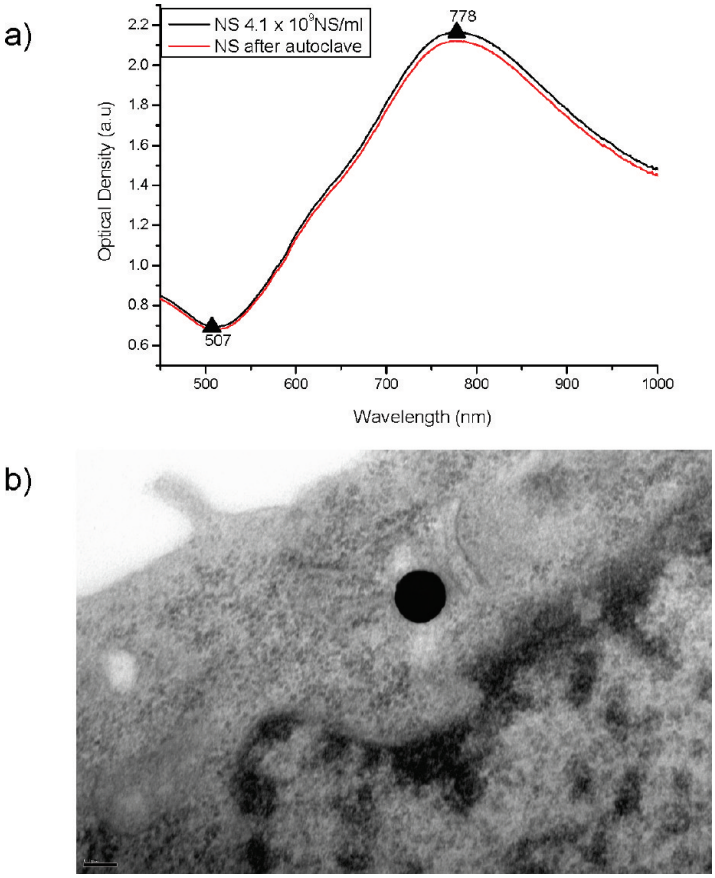

Figure 1. (a) Absorbance spectrum of NS with absorbance maximum in the NIR at 778 nm. (b) TEM images of NS inside NIH/3T3; image on the left showing a NS pair in the cytoplasm near the nuclear membrane (scale bar 0.2 μm).

in Raman measurements taken of whole cells and the SER spectra, with NS probing different locations in the cytosol, and demonstrate the use of functionalized NS for intracellular pH measurement.[35]

RESULTS AND DISCUSSION

Cellular Uptake of NS. The absorbance maximum and size of the NS used in this study were determined to be at 778 nm and 151 ± 5 nm as measured by UV−vis and scanning electron microscopy, respectively (Figure 1a,b). Before bringing in contact with cells, the particles were sterilized by autoclaving and the absorbance was checked and compared to nonsterilized NS. Autoclaving caused no changes to the absorbance of the NS solution, as shown in Figure 1a, confirming that the particles are still intact and their plasmon resonance remains unaltered. The sterile particles with a concentration of 6.9 pM were diluted to a concentration of 10 fM in DMEM growth media supplemented with 10% calf serum directly before incubation with NIH/3T3 fibroblast cells for 5 h. To the best of our knowledge, the uptake, toxicity, and fate of NS taken up into cells have not been studied. First, we investigated the uptake of NS in 3T3s in standard growth conditions and confirmed the inclusion of the bare gold NS by TEM microscopy (Figure 1b) in the vicinity of the nuclear membrane.[36,37] This proves that NS are taken up voluntarily inside the cells without the use of a transfecting agent.

Further, we examined whether NS are taken up *via* an active endocytotic uptake mechanism as has been reported by Rejman *et al.*, who found that 50−200 nm fluorescent latex beads were taken up by a clathrin-mediated process,[38] or by an unknown alternative mechanism. Therefore, we preincubated the cells with different buffers, leading to the inhibition of different endocytotic mechanisms, and incubated the cells with NS at a concentration of 10 fM in standard growth conditions with media containing 10% CS. The three preincubations cause cells to be either ATP-, cholesterol-, or potassium-depleted, allowing us to investigate the energy dependence of an active mechanism, inhibition of the formation of lipid rafts, and the interruption of clathrin-mediated uptake, respectively.[39,40] The NS incubations were conducted for 5 h (because we found this to be sufficient for introduction of small numbers of NS) before fixation and preparation for TEM sectioning and measurement. To obtain information about the differences of particle uptake, 100 sectioned cells were checked and particles counted. The thickness of the cell sections was 120 nm, and therefore, it was estimated that around 100 cell sections would statistically account for one NIH/3T3 cell of an average diameter of around 10 μm ± 20%. The NS amount per cell was then determined in accordance with these assumptions. We expected to find a decrease in particle uptake in one or more cases where fibroblast cells were deficient in compounds crucial for endocytotic uptake,[22] compared to the control experiment without separate treatment. The uptake of NS did not decrease at all (Figure 2a) and seems to be slightly increased for the cases where cells were depleted of ATP, cholesterol, and potassium. These findings indicate that these established endocytosis mechanisms are not solely responsible for NS internalization.

Previous reports have implicated serum protein adsorption in nanoparticle uptake,[1] and further incubation with NS in serum-free media over the same duration actually shows a large increase in NS uptake (Figure 2a), in the range of up to 6-fold. This observation rules out an endocytosis mechanism mediated by adsorption of serum proteins and suggests that the absence of serum proteins makes NS uptake more efficient.

In order to try and understand the NS uptake in more detail, we made further investigations with TEM to gain information about the uptake, fate, and localization of NS inside the cells. A magnification up to 33 000× allowed us to observe the close surrounding of the particles inside the cells. Of 67 sections with NS which we examined, we always found NS localized in the cytosol and observed that, while the particles can be found near the nuclear membrane, they are never

present in the nucleus. We show in Figure 3a−c particles which were incorporated in the presence of serum in the media; panel d is a representative image of a particle taken up in the absence of serum in the media. Figure 3a shows NS which were found free (not incorporated in a vesicle) in the cytosol—about 50% of the particles taken up in conditions with serum in the media can be found free inside the cells. NS can be also found in vesicles, probably lysosomes (Figure 3b), or coated by a layer (Figure 3c) 5−10 nm thick and of high density, similar to surrounding cytosolic proteins. We suspected that this might be a layer of serum proteins adsorbed to the particle, but when we examined NS which were incubated solely in growth media with serum after several hours, a similar coating could not be found (Supporting Information). On the basis of this evidence, it appears that the coating forms during or after entry to the cell, perhaps as a reaction to the foreign particle. In the case where NS were taken up by cells in serum-free media, TEM images show uncoated NS without vesicles (Figure 3d). This information is crucial for selecting the best condition for intracellular sensor development, where a free particle surface is desirable. It appears that the uptake mechanism allows the particles to merge with the membrane and pass through it without encapsulation. This explanation can be partly backed up by the findings of Roiter *et al.*, who reported that the curvature of lipid bilayers dropped onto smooth nanoparticles between 22 and 200 nm diameter does not promote membrane brakes.[41] As particles of sizes up to 100 nm are known to be taken up by active endocytosis,[1,21,42] we speculate a mechanism in which the particles merge with and pass through the membrane at areas of high membrane fluidity.[43] This would also explain the increased uptake in the cases of cholesterol depletion since cholesterol leads to increased membrane rigidity and also the increased uptake in serum-free media, where the particles display no adsorbed serum proteins and are therefore not led to protein receptors found in rigid lipid rafts.[39] We intend to carry out tracking experiments in live cells in order to further investigate the uptake mechanism.

We also conducted an experiment aimed at controlling the number of particles per cell by adjusting the concentration of NS, as can be seen in Figure 2b. Here we show in a very basic experiment the amount of particles taken up at 10, 150, and 300 fM NS concentrations in the growth media. Particle amounts were found to be taken up with linear behavior in the range of the observed concentrations. This leads to a very easy way to control particle loading into the cells and also confirms that around 1 out of 60 particles are taken up from solution in these particular conditions (although this ratio is likely to differ with different nanoparticles and cell types).

Cell Viability during NS Incubation. A range of 11 NS concentrations between 0 and 300 fM were prepared in growth media with serum. The NS were added to cells in 96-well plates seeded at 50% confluence the previous day and washed with PBS prior to NS treatment. The CellTiter-Blue fluorescence assay was used according to protocol at different time points up to 96 h after incubation.

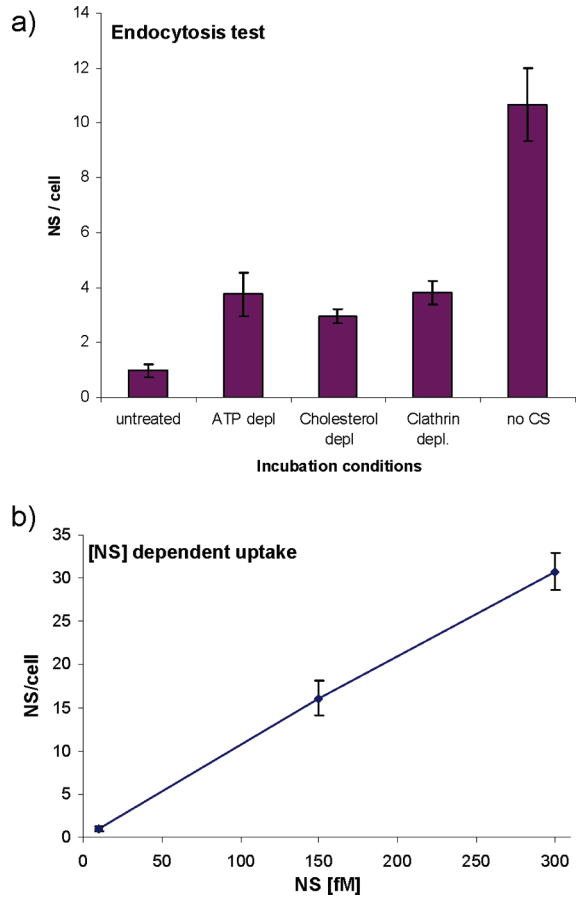

Figure 2. (a) Estimated amount of NS per cell according to particles found in 100 TEM sections. NS incubations for this test were conducted for 5 h with 10 fM NS in 10% CS containing media, except the condition with no CS on the right. The bars show the amount of NS (monomers, dimers) found in 100 cell sections. (b) Increase of NS in cells is proportional to the NS concentration during the incubation at normal growth conditions with 10% CS.

The results of the cell viability test in Figure 4 show that there is no difference between growth of NIH/3T3 cells at standard conditions without NS or incubated with different NS concentrations of up to 300 fM correlating to 1800 NS/cell. Figure 4 shows that fibroblast cells exhibit the same growth behavior, reaching the static phase after 2−3 days regardless of the presence of NS in the media. Hence, we assume that there are no detrimental effects on cell growth when cells are incubated with NS at the described conditions. In order to further ensure that there are no detrimental effects of NS incubation, we also assayed for molecular markers of cell death. We did this by measuring markers of apoptosis and necrosis at the lowest and highest NS concentrations detailed above. For the apoptosis test, an assay for caspases 3 and 7 was chosen as these proteases

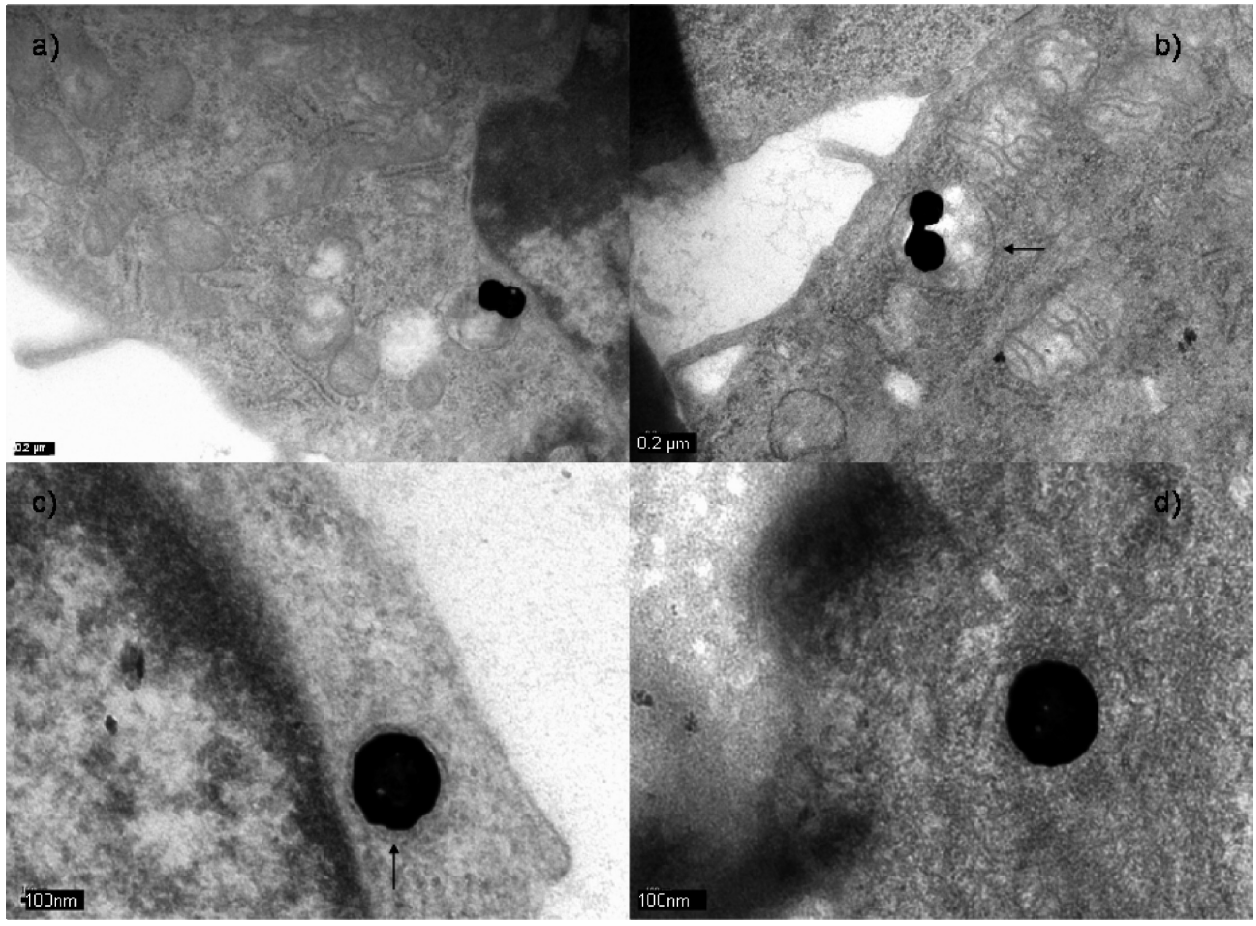

Figure 3. Set of TEM images of NS inside cells. Images a, b, and c are all of NS, which were incubated in media containing 10% CS and can be found either (a) free suspended in the cytosol (scale bar 0.2 µm), (b) taken up in oversized vesicles, or (c) surrounded by what might possibly be a dense coating of protein. (d) Representative NS which has been taken up during incubation without any CS in the growth media. None of the NS found in these conditions was surrounded by any kind of coating or vesicles inside the cells.

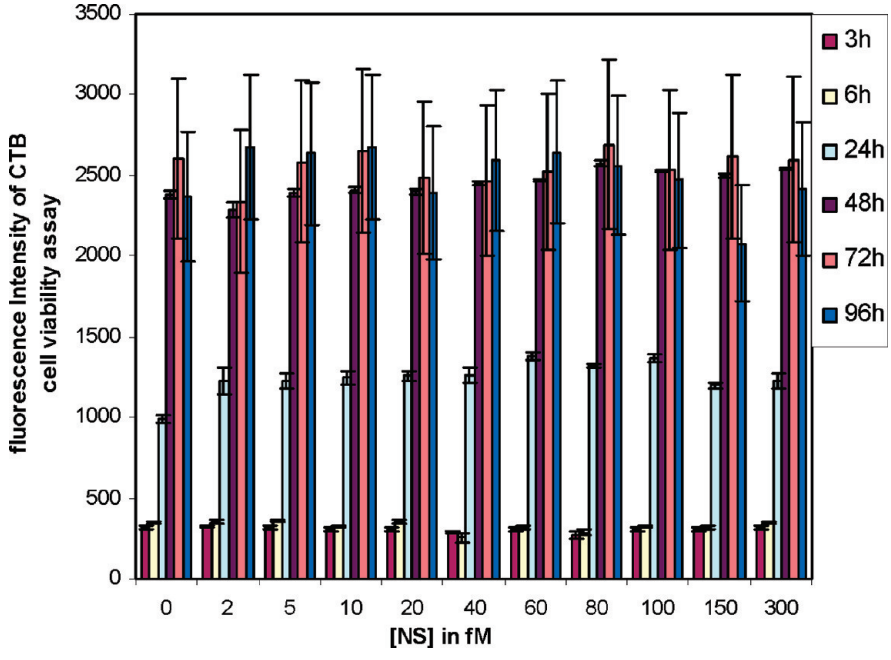

Figure 4. CellTiter-Blue cell viability test showing fluorescence signal strengths of cells incubated with varying NS concentrations of 0−300 fM at different time points up to 96 h. The intensity is normalized to the control and proportional to the cell population per well. Error bars depict single standard deviations of five replicates.

are among the first signals in the apoptosis cascade leading to imminent death of the cell. Figure 5a shows the results of this assay at 10 and 300 fM NS. The tests were conducted at intervals of 3, 6, 9, 12, and 24 h after the start of incubation, and in addition, a positive control was run incubating cells for 3 h with staurosporine, which has a known cytotoxic effect leading to apoptosis. It can be seen that the incubation with NS did not promote apoptosis at any time up to 24 h compared to the negative control of untreated NIH/3T3 fibroblasts. Therefore, we can assume that cells which have taken up NS do not undergo apoptosis on the time scale measured.

In order to investigate the possibility of NS-induced necrosis (potentially due to membrane disruption), an assay was used to probe for free

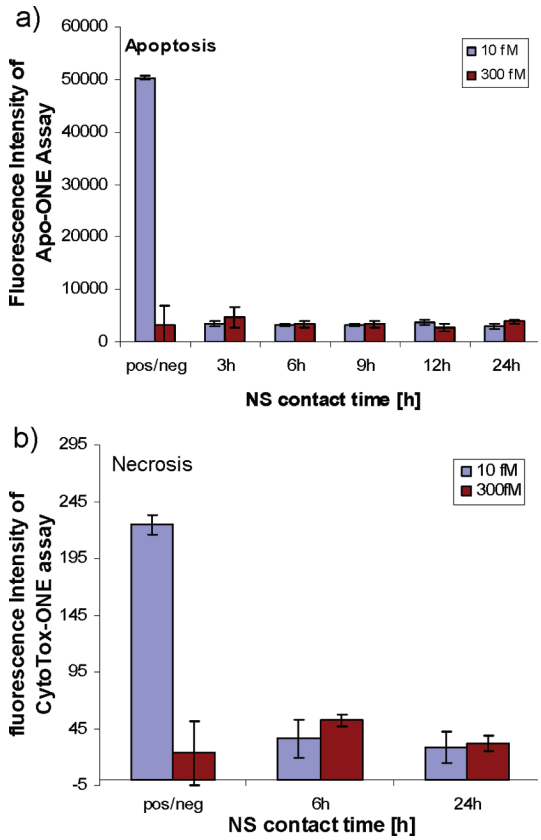

Figure 5. (a) Results of ApoONE homogeneous caspases 3/7 test for 10 fM (low) and 300 fM (high) NS concentrations incubated for up to 24 h. Positive control was incubated with 1 μm staurosporine for 3 h; negative controls were untreated cells. (b) Fluorescence results for CytoTox-ONE kit; positive control was obtained by lysing cells with provided buffer solution, and negative controls were untreated cells. Error bars in both measurements were standard deviations of five replicates.

lactase in the extracellular environment which would appear as a result of the release of intracellular components. For this assay, cells were incubated with the same two NS concentrations as above and tested at 6 and 24 h after the start of incubation. In this case, the positive control was a sample of cells treated for 30 min with lysis buffer, which leads to disintegration of the cells. Incubation with NS concentrations after 6 and 24 h did not show any increase in signal compared to the negative control with untreated cells. This supports the result that, as in the case of gold nanorods,[44] gold nanoshells have no cytotoxic effect on fibroblast cells.

Intracellular Surface-Enhanced Raman Spectroscopy with Nanoshells. The NS we have used in this work are designed to be excited with lasers in the NIR region, which have excellent transmittance through tissue. To date, these NS have been added to cells as a potential cancer therapy;[29,45] however, they also have potential use as transducer elements for surface-enhanced Raman spectroscopy.[35,46,47] We therefore demonstrate here the use of NS to acquire spectra from the intracellular environment of living and viable NIH/3T3s cells.

First, we have compared the differences between unenhanced Raman measurements collected using detached living NIH/3T3 cells and SERS spectra enhanced by intracellular NS of NIH/3T3 cells grown on quartz coverslips (UQG Ltd., Cambridge). In order to obtain a detectable bulk Raman spectrum, we measured 50 surface-detached single cells using a laser power of 50 mW for a 180 s acquisition time on each cell. SERS spectra were collected after locating the gold nanoparticle light scattering pattern and acquiring spectra for 5 s with 3 mW laser power at the sample. The SERS spectra were taken in several single living cells at different locations (Figure 6). Comparing the two different kinds of Raman measurements, we observed that some features are clearly visible in the bulk Raman as in the SERS spectra, such as the peak at around 1005 cm^{-1} for phenylalanine or the amide-III/β-sheet band at 1215 cm^{-1}.

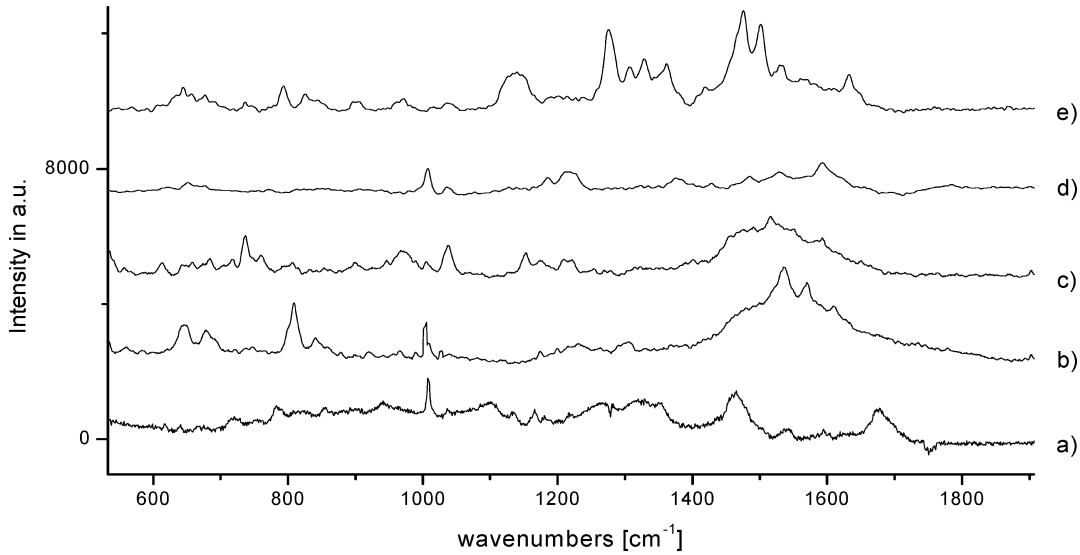

Figure 6. (a) Averaged Raman spectrum of 50 different NIH/3T3 fibroblast cells measured at a 785.32 nm excitation wavelength, 50 mW laser power at the sample for 180 s. (b–e) SER spectra taken by excitation of NS in different cells at the same wavelength with 5 s acquisition time and 3 mW laser power at the sample.

TABLE 1. Raman Assignment for Peaks of Bulk Raman Spectra of Single Cells (a), and the SERS Features of NS Inside Cells (b, c, d, e) of the Spectra in Figure 6

single cell		NS in different cells			
(a) (cm^{-1})	assignment for Raman features	(b) (cm^{-1})	(c) (cm^{-1})	(d) (cm^{-1})	(e) (cm^{-1})
640	C−C twist in tyrosine	646		642	644
675	C−S stretch in cysteine	678	684		
720	C−N stretch in lipid/adenine		736		737
783	DNA: O−P−O backbone stretch in thymine/cytosine				
825	DNA: O−P−O backbone stretch/out-of-plane ring breath in tyrosine				825
856	on-plane ring breathing mode in tyrosine/ C−C	848		850	
893	C−C skeletal stretch in protein		900	905	896
941	C−C skeletal stretch in protein		967		972
1008	symmetric ring breathing mode of phenylalanine	1005	1005	1007	1428
1036	C−H in-plane bending mode of phenylalanine		1037	1038	1036
1100	DNA: O−P−O backbone stretching				
1109	DNA: O−P−O backbone stretching				
	C−N stretch in polypeptide chains		1133	1138	1139
1166	C−C stretching in proteins	1174	1174		
1217	Amide III: beta-sheet	1216	1209	1214	1214
1266	Amide III:β-sheet/adenine/cytosine				1275
1329	guanine			1323	1329
1354	polynucleotide chain (DNA bases)				
	possible porphyrin stretches			1375	1366
1465	(ν(C═C) + ν(C− C) + ν(C═O · − · H)), chromophore			1485	1475
	aromatic ring stretches		1516		1511
1543	lipid stretches	1535		1528	1534
	tyrosine stretch	1570		1593	1570
1595	ring mode (adenine/guanine)				
1619	C═C bending in phenylalanine and tyrosine	1616			
1677	amide I:α-helix				

However, we see no DNA-related peaks in the SERS spectra; this is expected if, as shown above, NS are only found in the cytosol. Other peak assignments can be found in Table 1. We estimate the enhancement of the Raman signal of cytosolic compounds with NS to be 10^{10} compared to the single cell Raman measurements (Supporting Information).

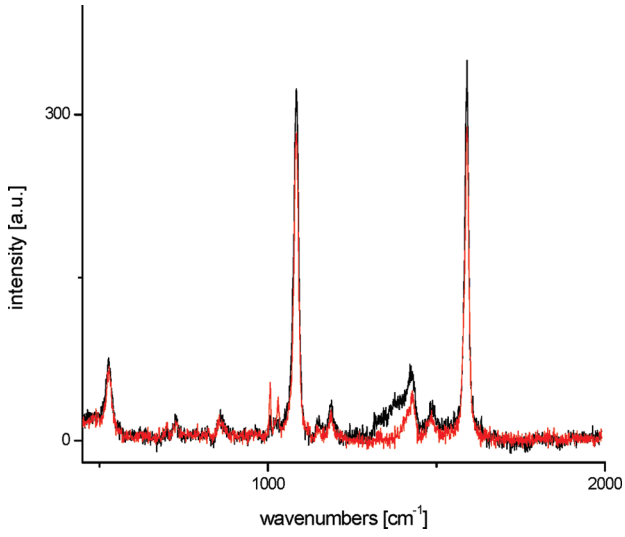

Figure 7. SER spectra of 4-mercaptobenzoic acid (4-MBA)-functionalized NS in NIH/3T3 fibroblast. Overlying spectra depict NS-4-MBA in solution (black) and inside NIH/3T3 cells determining the pH to be 7.4 and 6.5, respectively.

Although a much higher signal can clearly be acquired with NS inside the cells, the lack of specific information from the complex mix of biomolecules found in the cytoplasm would make it difficult to extract biologically relevant data using this technique. It is our opinion that the value of this technique lies in the development of SERS NS sensors that are made sensitive to intracellular conditions, like pH, redox potential, or specific protein concentrations by the addition of signaling probes. The use of 4-MBA-functionalized Au particles for intracellular pH determination has been shown by Kneipp *et al.*, where the particles were "probably located in lyzosomes".[42] For the use of a nanosensor, it is of high importance that surface functionalities remain intact while inside the cell and the spectra are not disturbed by signals originating from foreign molecules adhering to the sensor surface. We use 4-MBA-functionalized NS for this simple test as it is known to easily form self-assembled monolayers on Au surfaces.[35,48] The spectra (Figure 7a) of 4-MBA-NS inside cells and free in media do not show any obvious differences. The dominant features in the spectra are the aromatic ring breathing modes at 1081 and 1590 cm^{-1}. Other less intense features describe the S−C stretching mode of the thiol function at 527 cm^{-1}, different carboxyl modes at 860 cm^{-1} (d(COO^-)), 1150 cm^{-1} (C−COOH), and 1430 cm^{-1} (−COO^-),[35,48] which are all dependent on the pH of the surrounding solu-

tion. In the above shown spectra, the pH can be determined to be pH 7.4 for the particles in the growth media and pH 6.5 for the NS-4-MBA inside the cell (pH calibration data in Supporting Information) calculated from the peak ratios between the peak intensities at 1430 and 1700 cm^{-1}.

CONCLUSIONS

We have reported here the voluntary, controllable cellular uptake of single gold nanoshells, which is independent of the known endocytotic mechanisms investigated. We also demonstrated that cell viability is maintained in these conditions and that molecular markers of apoptosis or necrosis show no difference to control samples and therefore no detrimental effects on cellular metabolism. Further, we also demonstrated that the SPR properties of the gold nanoparticles can be used to acquire SER spectra probing the intracellular environment, and we have shown that SERS chemosensor signals can be obtained without interfering signals from intracellular compounds. Overall, we have shown that NS can be used as a viable and versatile platform for intracellular SERS nanosensors.

EXPERIMENTAL SECTION

All reagents were ordered from Sigma Aldrich if not stated otherwise and used without further purification.

Cell Culture: NIH/3T3 mouse fibroblast cells were cultured in Dulbeco's modified eagle medium (DMEM; Invitrogen, UK) supplemented with penicillin/streptomycin (10 000 units/mL), L-gluthamine (200 mM), and 10% heat-inactivated calf serum. Cells were seeded at around 50% confluence for the different experiments and incubated overnight at 37 °C and 5% CO_2.

NS Incubation: Before incubation, NS cells were washed with PBS three times, and afterward, media with the required NS concentration were put on the cells. Incubations (if not otherwise stated) were conducted for 5 h at standard incubation conditions.

For the following fluorescence assays, the signal was normalized to the background signal of cells grown over the same length of time covered in growth media. Errors were estimated by taking the standard deviation of five replicates.

For the cell viability test, the CellTiter-Blue (CTB) assay (Promega, UK) was used in a 96-well format. Cells were incubated with above stated growth media supplemented with NS (autoclaved after delivery, Nanospectra, US) at concentrations from 0 to 300 fM (approximately 0−1800 NS/cell, respectively). The CTB assay was conducted after 3, 6, 24, 48, 72, and 96 h according to protocol.

Apo-ONE homogeneous caspase-3/7 assay and CytoTox-ONE homogeneous membrane integrity assay (Promega, UK) were used to detect possible apoptosis and necrosis signals after incubation with 10 and 300 fM NS in culture media. Positive controls for apoptosis were incubated for 3 h with 1 μM of staurosporine in growth media.

For investigations of cellular uptake mechanism, cells were grown at standard conditions on resin beads and then preincubated for 1 h with PBS buffer containing NaN_3 (10 mM) and glucose (50 mM) for ATP depletion. A second buffer with methyl-β-cyclodextrin (10 mM) and a potassium-free buffer made up of HEPES (50 mM), NaCl (100 mM), and $MgCl_2$ (1 mM) were used for cholesterol depletion and potassium depletion, respectively. Buffers were sterile filtered, and cells were incubated in separate flasks for 1 h. Subsequently, the cells were washed with PBS and incubated with NS in media at a concentration of 10 fM. After 5 h of incubation, the media were taken out and the cells were washed with PBS and fixed in 1% glutaraldehyde in PBS. For TEM measurements, the samples were dehydrated in acetone and stained with osmium tetroxide.

SERS measurements were done with cells grown on quartz coverslips (0.2 mm, UQG Ltd., England) and incubated with media containing 300 fM of either bare or functionalized NS incubated in serum-free media for 5 h.

Fluorescence Measurements: Assays were run in 96-well plates, measured with a POLARstar OPTIMA microplate reader, and signals were normalized to the intensity of wells containing untreated cells. The appropriate filter and light source setups recommended in the protocols were used.

Transmission Electron Microscopy: Processed cells on resin beads were transferred into resin for sectioning. Sections of 120 nm thickness were taken and put on a TEM grid for measurement. Each section contained between 50 and 100 cells. Acquistions were made with a CM120 Biotwin (Philips) transmission electron microscope connected to a digital camera.

Nanoshell Functionalization: For the functionalization of sterile NS with 4-mercaptobenzoic acid, 300 μL of a NS solution of 6.9 pM was added to 1 μM 4-MBA in (10 uL) and incubated overnight at room temperature. Excess 4-MBA was washed off by centrifugation, and the sample was washed a further two times in double distilled H_2O.

Surface-Enhanced Raman Spectroscopy: An inverted Raman system built around a self-constructed microscope was used to evaluate the cellular samples. Briefly, a temperature-stabilized diode laser operating at 785 nm (a circularized laser Diode, Sanyo DL-7140-201s up to 80 mW power) is expanded and introduced *via* a holographic notch filter (HNF, Tydex notch-4) into an inverted microscope and passed to the sample *via* a 350 NA 0.9 oil immersion objective. The backscattered Raman light is collected by the same objective and passed through the HNF. The Raman signal is then reflected by the dichroic mirror and imaged onto a 200 lm confocal aperture. Finally, the beam is imaged onto the spectrograph (Triax 550 Jobin Yvon). This spectrograph employs a 300 lines/mm grating and is equipped with a CCD camera (Symphony OE STE Jobin Yvon) for detection of the Raman spectrum. The Raman signal is imaged onto the CCD by making use of a lens placed at a distance equal to its focal length ($f = 80$ mm) from the slit of the spectrograph. Laser power used during the measurements for bulk Raman studies on detached single cells was 50 mW and 180 s acquisition time. Spectra of 50 cells were averaged and water-background-corrected. Bare and 4-MBA-functionalized NS inside cells were detected by looking out for bright scattering events while moving the laser beam through the cells, and NS-based SERS measurements were obtained with 3 mW laser power at the sample and 5 s acquisition time.

Acknowledgment. The authors thank the UK Engineering and Physical Sciences Research Council and EaStChem for funding and Scottish Microelectronics Centre for the use of SEM. K.D. is a Royal Society−Wolfson Merit Award Holder. We thank S. Mitchell at the Institute of Molecular Plant Sciences for his valuable advice and help on matters of cell TEM.

Supporting Information Available: Sample TEM images of NS after overnight incubation in DMEM growth media supplemented with 10% CS; calibration curve of pH sensor and estimation of enhancement factor. This material is available free of charge *via* the Internet at http://pubs.acs.org.

REFERENCES AND NOTES

1. Chithrani, B. D.; Ghazani, A. A.; Chan, W. C. W. Determining the Size and Shape Dependence of Gold Nanoparticle Uptake into Mammalian Cells. *Nano Lett.* **2006**, *6*, 662–668.

2. Cognet, L.; Tardin, C.; Boyer, D.; Choquet, D.; Tamarat, P.; Lounis, B. Single Metallic Nanoparticle Imaging for Protein Detection in Cells. *Proc. Natl. Acad. Sci. U.S.A.* **2003**, *100*, 11350–11355.
3. Hu, Y.; Litwin, T.; Nagaraja, A. R.; Kwong, B.; Katz, J.; Watson, N.; Irvine, D. J. Cytosolic Delivery of Membrane-Impermeable Molecules in Dendritic Cells Using pH-Responsive Core−Shell Nanoparticles. *Nano Lett.* **2007**, *7*, 3056–3064.
4. Jarvis, R. M.; Law, N.; Shadi, I. T.; O'Brien, P.; Lloyd, J. R.; Goodacre, R. Surface-Enhanced Raman Scattering from Intracellular and Extracellular Bacterial Locations. *Anal. Chem.* **2008**, *80*, 6741–6746.
5. Ma, L. L.; Feldman, M. D.; Tam, J. M.; Paranjape, A. S.; Cheruku, K. K.; Larson, T. A.; Tam, J. O.; Ingram, D. R.; Paramita, V.; Villard, J. W.; *et al.* Small Multifunctional Nanoclusters (Nanoroses) for Targeted Cellular Imaging and Therapy. *ACS Nano* **2009**, *3*, 2686–2696.
6. Harush-Frenkel, O.; Rozentur, E.; Benita, S.; Altschuler, Y. Surface Charge of Nanoparticles Determines Their Endocytic and Transcytotic Pathway in Polarized MDCK Cells. *Biomacromolecules* **2008**, *9*, 435–443.
7. Dubach, J. M.; Harjes, D. I.; Clark, H. A. Fluorescent Ion-Selective Nanosensors for Intracellular Analysis with Improved Lifetime and Size. *Nano Lett.* **2007**, *7*, 1827–1831.
8. Kumar, S.; Harrison, N.; Richards-Kortum, R.; Sokolov, K. Plasmonic Nanosensors for Imaging Intracellular Biomarkers in Live Cells. *Nano Lett.* **2007**, *7*, 1338–1343.
9. El-Sayed, I. H.; Huang, X.; El-Sayed, M. A. Surface Plasmon Resonance Scattering and Absorption of Anti-EGFR Antibody Conjugated Gold Nanoparticles in Cancer Diagnostics: Applications in Oral Cancer. *Nano Lett.* **2005**, *5*, 829–834.
10. Gobin, A. M.; Lee, M. H.; Halas, N. J.; James, W. D.; Drezek, R. A.; West, J. L. Near-Infrared Resonant Nanoshells for Combined Optical Imaging and Photothermal Cancer Therapy. *Nano Lett.* **2007**, *7*, 1929–1934.
11. Hirsch, L. R.; Gobin, A. M.; Lowery, A. R.; Tam, F.; Drezek, R. A.; Halas, N. J.; West, J. L. Metal Nanoshells. *Ann. Biomed. Eng.* **2006**, *34*, 15–22.
12. Liu, C.; Mi, C. C.; Li, B. Q. Energy Absorption of Gold Nanoshells in Hyperthermia Therapy. *IEEE Trans. Nanobiosci.* **2008**, *7*, 206–14.
13. Loo, C.; Lowery, A.; Halas, N.; West, J.; Drezek, R. Immunotargeted Nanoshells for Integrated Cancer Imaging and Therapy. *Nano Lett.* **2005**, *5*, 709–711.
14. Bhirde, A. A.; Patel, V.; Gavard, J.; Zhang, G.; Sousa, A. A.; Masedunskas, A.; Leapman, R. D.; Weigert, R.; Gutkind, J. S.; Rusling, J. F. Targeted Killing of Cancer Cells *In Vivo* and *In Vitro* with EGF-Directed Carbon Nanotube-Based Drug Delivery. *ACS Nano* **2009**, *3*, 307–316.
15. Maynard, A. D.; Aitken, R. J.; Butz, T.; Colvin, V.; Donaldson, K.; Oberdorster, G.; Philbert, M. A.; Ryan, J.; Seaton, A.; Stone, V.; Tinkle, S. S.; Tran, L.; Walker, N. J.; Warheit, D. B. Safe Handling of Nanotechnology. *Nature* **2006**, *444*, 267–269.
16. Muller, J.; Decordier, I.; Hoet, P. H.; Lombaert, N.; Thomassen, L.; Huaux, F.; Lison, D.; Kirsch-Volders, M. Clastogenic and Aneugenic Effects of Multi-wall Carbon Nanotubes in Epithelial Cells. *Carcinogenesis* **2008**, *29*, 427–433.
17. Poland, C. A.; Duffin, R.; Kinloch, I.; Maynard, A.; Wallace, W. A. H.; Seaton, A.; Stone, V.; Brown, S.; MacNee, W.; Donaldson, K. Carbon Nanotubes Introduced into the Abdominal Cavity of Mice Show Asbestos-like Pathogenicity in a Pilot Study. *Nat. Nano* **2008**, *3*, 423–428.
18. Dumortier, H.; Lacotte, S.; Pastorin, G.; Marega, R.; Wu, W.; Bonifazi, D.; Briand, J.-P.; Prato, M.; Muller, S.; Bianco, A. Functionalized Carbon Nanotubes Are Non-cytotoxic and Preserve the Functionality of Primary Immune Cells. *Nano Lett.* **2006**, *6*, 3003.
19. Talley, C. E.; Jusinski, L.; Hollars, C. W.; Lane, S. M.; Huser, T. Intracellular pH Sensors Based on Surface-Enhanced Raman Scattering. *Anal. Chem.* **2004**, *76*, 7064–7068.
20. Tang, H.-W.; Yang, X. B.; Kirkham, J.; Smith, D. A. Probing Intrinsic and Extrinsic Components in Single Osteosarcoma Cells by Near-Infrared Surface-Enhanced Raman Scattering. *Anal. Chem.* **2007**, *79*, 3646–3653.
21. Shukla, R.; Bansal, V.; Chaudhary, M.; Basu, A.; Bhonde, R. R.; Sastry, M. Biocompatibility of Gold Nanoparticles and Their Endocytotic Fate Inside the Cellular Compartment: A Microscopic Overview. *Langmuir* **2005**, *21*, 10644–10654.
22. Kam, N. W. S.; Liu, Z.; Dai, H. Carbon Nanotubes as Intracellular Transporters for Proteins and DNA: An Investigation of the Uptake Mechanism and Pathway. *Angew. Chem., Int. Ed.* **2006**, *45*, 577–581.
23. Jin, H.; Heller, D. A.; Sharma, R.; Strano, M. S. Size-Dependent Cellular Uptake and Expulsion of Single-Walled Carbon Nanotubes: Single Particle Tracking and a Generic Uptake Model for Nanoparticles. *ACS Nano* **2009**, *3*, 149–158.
24. Hirsch, L. R.; Jackson, J. B.; Lee, A.; Halas, N. J.; West, J. L. A Whole Blood Immunoassay Using Gold Nanoshells. *Anal. Chem.* **2003**, *75*, 2377–2381.
25. Pham, T.; Jackson, J. B.; Halas, N. J.; Lee, T. R. Preparation and Characterization of Gold Nanoshells Coated with Self-Assembled Monolayers. *Langmuir* **2002**, *18*, 4915–4920.
26. Oldenberg, S. J.; Averitt, R. D.; Westcott, S. L.; Halas, N. J. Nanoengineering of Optical Resonances. *Chem. Phys. Lett.* **1998**, *288*, 243–247.
27. Alvarez-Puebla, R. A.; Ross, D. J.; Nazri, G. A.; Aroca, R. F. Surface-Enhanced Raman Scattering on Nanoshells with Tunable Surface Plasmon Resonance. *Langmuir* **2005**, *21*, 10504–10508.
28. Bardhan, R.; Grady, N. K.; Cole, J. R.; Joshi, A.; Halas, N. J. Fluorescence Enhancement by Au Nanostructures: Nanoshells and Nanorods. *ACS Nano* **2009**, *3*, 744–752.
29. Gobin, A. M.; Lee, M. H.; Halas, N. J.; James, W. D.; Drezek, R. A.; West, J. L. Near-Infrared Resonant Nanoshells for Combined Optical Imaging and Photothermal Cancer Therapy. *Nano Lett.* **2007**, *7*, 1929–1934.
30. Lassiter, J. B.; Aizpurua, J.; Hernandez, L. I.; Brandl, D. W.; Romero, I.; Lal, S.; Hafner, J. H.; Nordlander, P.; Halas, N. J. Close Encounters between Two Nanoshells. *Nano Lett.* **2008**, *8*, 1212–1218.
31. Nehl, C. L.; Grady, N. K.; Goodrich, G. P.; Tam, F.; Halas, N. J.; Hafner, J. H. Scattering Spectra of Single Gold Nanoshells. *Nano Lett.* **2004**, *4*, 2355–2359.
32. Jain, P. K.; El-Sayed, M. A. Universal Scaling of Plasmon Coupling in Metal Nanostructures: Extension from Particle Pairs to Nanoshells. *Nano Lett.* **2007**, *7*, 2854–2858.
33. Heck, K. N.; Janesko, B. G.; Scuseria, G. E.; Halas, N. J.; Wong, M. S. Observing Metal-Catalyzed Chemical Reactions *In Situ* Using Surface-Enhanced Raman Spectroscopy on Pd−Au Nanoshells. *J. Am. Chem. Soc.* **2008**, *130*, 16592–16600.
34. Levin, C. S.; Bishnoi, S. W.; Grady, N. K.; Halas, N. J. Determining the Conformation of Thiolated Poly(ethylene glycol) on Au Nanoshells by Surface-Enhanced Raman Scattering Spectroscopic Assay. *Anal. Chem.* **2006**, *78*, 3277–3281.
35. Bishnoi, S. W.; Rozell, C. J.; Levin, C. S.; Gheith, M. K.; Johnson, B. R.; Johnson, D. H.; Halas, N. J. All-Optical Nanoscale pH Meter. *Nano Lett.* **2006**, *6*, 1687–1692.
36. Marquis, B. J.; Love, S. A.; Braun, K. L.; Haynes, C. L. Analytical Methods To Assess Nanoparticle Toxicity. *Analyst* **2009**, *134*, 425–439.
37. Verma, A.; Uzun, O.; Hu, Y.; Hu, Y.; Han, H.-S.; Watson, N.; Chen, S.; Irvine, D. J.; Stellacci, F. Surface-Structure-Regulated Cell-Membrane Penetration by Monolayer-Protected Nanoparticles. *Nat. Mater.* **2008**, *7*, 588–595.
38. Rejman, J.; Oberle, V.; Zuhorn, I. S.; Hoekstra, D. Size-Dependent Internalization of Particles *via* the Pathways of Clathrin- and Caveolae-Mediated Endocytosis. *Biochem. J.* **2004**, *377*, 159–169.
39. Nabi, I. R.; Le, P. U. Caveolae/Raft-Dependent Endocytosis. *J. Cell Biol.* **2003**, *161*, 673–677.

40. Anderson, R. G. W. Multiple Endocytic Pathways. *J. Invest. Dermatol.* **1992**, *99*, 7S–9S.
41. Roiter, Y.; Ornatska, M.; Rammohan, A. R.; Balakrishnan, J.; Heine, D. R.; Minko, S. Interaction of Nanoparticles with Lipid Membrane. *Nano Lett.* **2008**, *8*, 941–944.
42. Kneipp, J.; Kneipp, H.; McLaughlin, M.; Brown, D.; Kneipp, K. *In Vivo* Molecular Probing of Cellular Compartments with Gold Nanoparticles and Nanoaggregates. *Nano Lett.* **2006**, *6*, 2225–2231.
43. Eggeling, C.; Ringemann, C.; Medda, R.; Schwarzmann, G.; Sandhoff, K.; Polyakova, S.; Belov, V. N.; Hein, B.; von Middendorff, C.; Schonle, A.; Hell, S. W. Direct Observation of the Nanoscale Dynamics of Membrane Lipids in a Living Cell. *Nature* **2009**, *457*, 1159–1162.
44. Alkilany, A. M.; Nagaria, P. K.; Hexel, C. J.; Shaw, T. J.; Murphy, C. J.; Wyatt, M. D. Cellular Uptake and Cytotoxicity of Gold Nanorods: Molecular Origin of Cytotoxicity and Surface Effects. *Small* **2009**, *5*, 701–708.
45. Lal, S.; Clare, S. E.; Halas, N. J. Nanoshell-Enabled Photothermal Cancer Therapy: Impending Clinical Impact. *Acc. Chem. Res.* **2008**, *41*, 1842–1851.
46. Jackson, J. B.; Halas, N. J. Surface-Enhanced Raman Scattering on Tunable Plasmonic Nanoparticle Substrates. *Proc. Natl. Acad. Sci. U.S.A.* **2004**, *101*, 17930–17935.
47. Talley, C. E.; Jackson, J. B.; Oubre, C.; Grady, N. K.; Hollars, C. W.; Lane, S. M.; Huser, T. R.; Nordlander, P.; Halas, N. J. Surface-Enhanced Raman Scattering from Individual Au Nanoparticles and Nanoparticle Dimer Substrates. *Nano Lett.* **2005**, *5*, 1569–1574.
48. Kneipp, J.; Kneipp, H.; Wittig, B.; Kneipp, K. One- and Two-Photon Excited Optical pH Probing for Cells Using Surface-Enhanced Raman and Hyper-Raman Nanosensors. *Nano Lett.* **2007**, *7*, 2819–2823.